

RESEARCH PAPER

## Hydrogen Evolution from Catalytic Hydrolysis of $\text{NaBH}_4$ : Comparative Study between the Catalytic Activity of $\text{TiO}_2$ Nanotubes with Various Arrangements

Neda Gilani<sup>1,2,\*</sup>, Javad Vahabzadeh Pasikhani<sup>2</sup>, Mahmood akbari<sup>2</sup>, Parisa Tafazoli Motie<sup>2</sup>

<sup>1</sup> Department of Chemical Engineering, University of Guilan, Rasht, Iran

<sup>2</sup> Fouman Faculty of Engineering, Collenge of Engineering, University of Tehran, Iran

### ARTICLE INFO

#### Article History:

Received 21 November 2018

Accepted 13 April 2019

Published 01 July 2019

#### Keywords:

Catalytic Hydrolysis

Disordered Filaments  $\text{TiO}_2$

Nanotubes

Free-Standing  $\text{TiO}_2$  Nanotubes

Hydrogen Generation

Sodium Borohydride

### ABSTRACT

Nowadays, a lot of efforts have been applied to find an appropriate catalyst for generating hydrogen from  $\text{NaBH}_4$ . Hence in the current study, various nanostructures of  $\text{TiO}_2$  were employed to obtain an insight into how the different support catalysts effect on the hydrolysis rate of  $\text{NaBH}_4$ . For this aim, disordered filaments (DF-NTs) and ordered free-standing  $\text{TiO}_2$  nanotubes (FS-NTs) were fabricated via hydrothermal and chemical-assisted two-step anodization methods, respectively. The physical and chemical features of catalysts were analyzed using FESEM, XRD, FTIR and BET analysis, respectively. The results showed,  $\text{TiO}_2$  itself has catalytic activity and the  $\text{H}_2$  generation rate by FS-NTs was 1.67 and 5.26 times more than the generation rate by DF-NTs and spherical  $\text{TiO}_2$  nanoparticles, respectively. This premier catalytic behavior of FS-NTs can be ascribed to its high surface area ( $112.77 \text{ m}^2/\text{g}$ ) and ordered arrangement of the nanotubes which allows reagents to be easily transferred to the active sites. The kinetic study revealed that hydrolysis of  $\text{NaBH}_4$  using the catalyst of FS-TNs is a first-order reaction regarding catalyst amount, while it is a zero-order reaction regarding the  $\text{NaBH}_4$  level. Moreover, the reusability results exhibited that FS-TNs has good durability and performance even up to the Fifth run.

### How to cite this article

Gilani N, Vahabzadeh Pasikhani J, Akbari M, Tafazoli Motie P. Hydrogen Evolution from Catalytic Hydrolysis of  $\text{NaBH}_4$ : Comparative Study between the Catalytic Activity of  $\text{TiO}_2$  Nanotubes with Various Arrangements. J Nanostruct, 2019; 9(3): 588-599. DOI: 10.22052/JNS.2019.03.020

### INTRODUCTION

Finding a suitable alternative of fossil fuel resources as an energy source is a main concern in the 21st century as the termination of fossil fuels resources, increasing environmental pollution and energy shortages [1-3]. In this context, hydrogen is considered to be one of the proper alternative candidates for future energy because of its high energy density and copious sources [4,5]. Presently, the most hydrogen is prepared by using natural gas steam reforming which consumes energy and creates large greenhouse gas emissions, mainly, carbon dioxide [6,7]. Therefore, expanding efforts have been recently done to

search for appropriate hydrogen storage materials. In recent years, sodium borohydride ( $\text{NaBH}_4$ ) has been taken into account as an attractive candidate for solid hydrogen storage materials owing to its high hydrogen content (10.8 wt% capacity), nontoxicity, non-flammable properties, pure hydrogen production and good stability in alkaline solutions [8,9]. Also, the byproduct corresponding to the sodium borohydride hydrolysis, i.e. sodium metaborate ( $\text{NaBO}_2$ ), is eco-friendly and can be recycled as the raw material for regeneration to  $\text{NaBH}_4$  [10]. Sodium borohydride can be classified as both a complex metal hydride and a chemical hydride as it can generate hydrogen in two

\* Corresponding Author Email: [gilani.chem@gmail.com](mailto:gilani.chem@gmail.com)

manners: thermolysis, where the stored hydrogen is set free by heating, and hydrolysis, where the stored hydrogen is released through reaction with water [11,12]. Since the thermolysis process requires high temperature, the sodium borohydride hydrolysis has been preferentially used to generate hydrogen [4]. Notwithstanding H<sub>2</sub> can be generated from sodium borohydride, the low hydrogen productivity of NaBH<sub>4</sub> at room temperature is regarded as a key problem to its commercialization, resulting from the low solubility of NaBH<sub>4</sub> and NaBO<sub>2</sub> byproduct in highly basic solution [13]. Hence to overcome this problem, suitable catalysts are needed to accelerate the NaBH<sub>4</sub> hydrolysis for H<sub>2</sub> generation in a more efficient way as follows [14]:



To date, noble metal-based catalysts (Au, Pt, Ru and Rh) are observed to be the most effective catalysts for hydrolyzing NaBH<sub>4</sub> [15-17]. However, the high cost of limited noble metal resources makes practical application undefendable [18]. Some low cost non-noble metals, such as Cu, Ni, Fe and Co, have been examined widely towards NaBH<sub>4</sub> hydrolysis because of their excellent physical and chemical properties [19-21]. However, the main drawback of the use of such non-noble metals is their agglomeration because of high surface energy involving in the exothermic reduction procedure, leads to a significant loss of catalytic activity [4]. Furthermore, the strong adsorption of resulted NaBO<sub>2</sub> byproducts on the catalytic surface leads to a dramatic loss of activity only after a few operative cycles [22]. A facile strategy to solve these problems is to find an appropriate supporting metal catalyst [16,23]. A suitable supporting material not only buttresses the active materials but also provides a large specific surface area along with the chance of better dispersion of the active phases [24]. Amongst diverse materials, TiO<sub>2</sub> is extensively applied as an alternative supporting material because of its unique chemical and physical features, exceptional stability, low price, nontoxicity and abundance [25,26]. Also, it is worth noting that there are two kinds of acid sites on the surfaces of TiO<sub>2</sub>: Brønsted-acid sites (surface-bound hydroxyl group i.e. Ti-OH) and Lewis-acid sites (exposed Ti<sup>iii+</sup> cation) [27,28]. Since NaBH<sub>4</sub> hydrolysis can be catalyzed by an acid [29,30], so TiO<sub>2</sub> can employ as an ideal supported metal catalyst for this reaction. Based on researchers' studies, two key parameters are found

to significantly affect catalytic performance during NaBH<sub>4</sub> hydrolysis. These parameters are the surface area and adsorption capacity [21,31]. In comparison with different TiO<sub>2</sub> nanostructures, TiO<sub>2</sub> nanotubes encompass many benefits such as single-step synthesis, providing great specific surface area, and facilitate the transport of reagents to reactive sites [17, 32]. To date, there are various methods for fabrication of TiO<sub>2</sub> nanotubes with diverse arrangements. Generally, disordered filaments of TiO<sub>2</sub> nanotubes are synthesized by hydrothermal method while extremely ordered TiO<sub>2</sub> nanotube arrays are synthesized through the anodization process [33]. In addition, oriented free-standing TiO<sub>2</sub> nanotube arrays can be achieved by separating the aligned anodic TiO<sub>2</sub> nanotubes from the metallic Ti substrate [34]. Based on our earlier study, catalytic activities of TiO<sub>2</sub> nanotubes are affected not only by their structure but also strongly by their morphology and arrangement [35]. According to our knowledge, however, no systematic study has been reported until now, that would undertake efforts to find the influence of different TiO<sub>2</sub> nanotubes arrangement as a supporting catalyst on NaBH<sub>4</sub> hydrolysis. In addition, it still lacks a comprehensive study which compares the catalytic behavior of disordered filaments of TiO<sub>2</sub> nanotubes with that of free-standing TiO<sub>2</sub> nanotube arrays especially in generating hydrogen from NaBH<sub>4</sub>.

Therefore in the present work, the catalytic activities of different TiO<sub>2</sub> nanotubes arrangements were investigated systematically for the first time. As the main novelty of this work, the catalytic activity of disordered filaments and ordered free-standing TiO<sub>2</sub> nanotubes in hydrogen generation from NaBH<sub>4</sub> hydrolysis were examined and compared. Moreover, as an original contribution of this work, the kinetic study of the catalytic hydrolysis of NaBH<sub>4</sub> over free-standing TiO<sub>2</sub> nanotubes was performed. In addition, in the current study, tuning the arrangement of TiO<sub>2</sub> nanotubes by chemical-assisted two-step anodization process was employed as a simple and facile route to enhance the hydrogen generation rate from catalytic hydrolysis of NaBH<sub>4</sub>.

## MATERIALS AND METHODS

### *Preparation disordered filaments of TiO<sub>2</sub> nanotubes*

Disordered filaments of TiO<sub>2</sub> nanotubes (DF-NTs) were prepared through an alkaline hydrothermal treatment. First, 2 g of commercial TiO<sub>2</sub> powder (P25, Evonik, Germany) was poured

in 100 ml of concentrated caustic NaOH solution (10 M) while stirring for 30 min. subsequently, the mixture was ultrasonicated for 30 min at ambient temperature to become homogenizer. Following the homogenized suspension was transferred to a Teflon-lined autoclave. The obtained solution was then heated at 150 °C under static condition for 48 h. The resulting white precipitates were rinsed with 0.1 M HCl solution and distilled water repeatedly until the solution pH entered near neutral pH. The final output was centrifuged, dried at 80 °C, and annealed for 2 h at 450 °C.

*Fabrication free-standing TiO<sub>2</sub> nanotube arrays*

Free-standing TiO<sub>2</sub> nanotube arrays (FS-NTs) were synthesized through chemical-assisted two-step anodization procedure in a two-electrode configuration with the Ti sheet as both anode and cathode. First, Ti sheet was degreased and cleaned by immersion in acetone, ethanol and deionized water for 10 min during each step. After drying, to obtain a completely smooth and sleek surface, the chemical polishing process was taken place in a solution containing nitric acid 65% and hydrofluoric acid 40% with a volume ratio of 3:1 for 2 min. Ethylene glycol with 0.5 wt.% ammonium fluoride and 2 vol% deionized water was used as the electrolyte. The first-step anodization started with the growth of TiO<sub>2</sub> nanotubes on Ti sheet with a constant voltage of 50 V for 1.5 hours at room temperature. The as-prepared TiO<sub>2</sub> nanotubes were then removed by acid treating process via diluted hydrofluoric acid to expose the substrate. Subsequently, the etched Ti substrate was anodized for the second time in the same

condition as the first step for 12 h. After completing the second anodization, the voltage was gradually decreased manually from adjusted potential to 10 V, over several seconds. Subsequently, the fabricated TiO<sub>2</sub> nanotubes layer was separated using ultrasonic treatment in methanol solution to achieve free-standing TiO<sub>2</sub> nanotubes. Afterward, to obtain a crystalline structure, the annealing of free-standing TiO<sub>2</sub> nanotubes was done for 2 h at 450 °C.

*Catalysts characterization*

The fabricated catalysts were analyzed using an X-ray diffractometer (XRD, Philips X’Pert Pro X-ray diffractometer, Germany) to obtain crystallographic information. The XRD patterns were recorded by means of Cu Kα radiation (the wavelength is 1.54 Å) in the 2θ range of 10-80. The surface morphologies, structural characteristics and elements present in the as-prepared catalysts were examined using a field-emission scanning electron microscope (FESEM, TESCAN MIRA3-XMU, Czech Republic) with an energy dispersive spectrometry (EDS) detector. To determine the functional groups available in the catalysts, the Fourier transform infrared analysis (FTIR; Bruker alpha-2000, USA) was performed over a wavenumber range of 500-4000 cm<sup>-1</sup>. The BET analysis of the catalysts was studied by means of a micrometer ASAP 2000 (USA). The BET (Brunauer-Emmet-Teller) method measures the specific surface area and the pore volume. Furthermore, the average pore diameter was estimated from adsorption isotherms by Barrette Joynere Halenda (BJH) analysis. The principle corresponding this

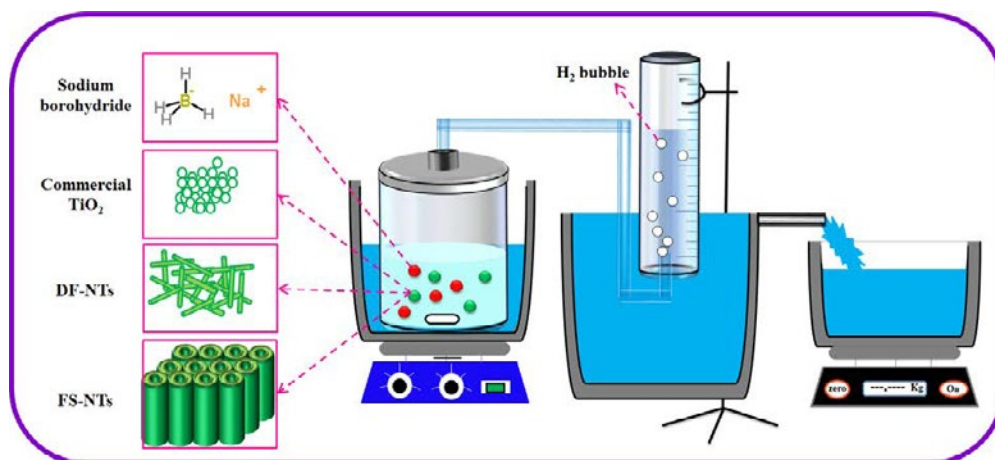


Fig. 1. Schematic corresponding to the experimental setup for generating hydrogen.

technique is on the basis of multiple points of nitrogen gas isothermal adsorptions-desorption.

*Hydrogen production*

The catalytic behaviors of the as-synthesized catalysts were investigated through hydrolyzing sodium borohydride solution. Fig. 1 indicates the typical experimental setup of producing hydrogen. The detailed procedure is as following: 10 mL NaBH<sub>4</sub> solution (containing 5 wt% NaBH<sub>4</sub> and 1.5 wt% NaOH) was poured into a sealed flask and placed in the thermostatic water-bath maintained at 30 °C. A water bath was utilized to keep the system under isothermal condition (30 °C). Then 10 mg of as-prepared catalysts were poured in a sealed reaction flask. The reaction proceeded at a stirring rate of 800 rpm and the concentration of hydrogen generated with time was measured

immediately. The volume of hydrogen generated was determined by water displacement method, where the hydrogen volume was equal to the displaced water whose weight was recorded by a balance. The rate of hydrogen generation and the factors affecting the the catalyst activity were examined. At the end of the reaction, the catalyst was retained through filtration, washed thoroughly and dried at 60 °C for 10 h. Then the reusability experiment was repeated for 5 cycles.

**RESULTS AND DISCUSSION**

*Characterization morphology*

Fig. 2 represents the FESEM photographs of commercial TiO<sub>2</sub> powder, DF-NTs and FS-NTs, respectively. As presented in Fig. 2(a), TiO<sub>2</sub> nanopowder has a non-uniform granular shape. After hydrothermal treatment, the DF-NTs are

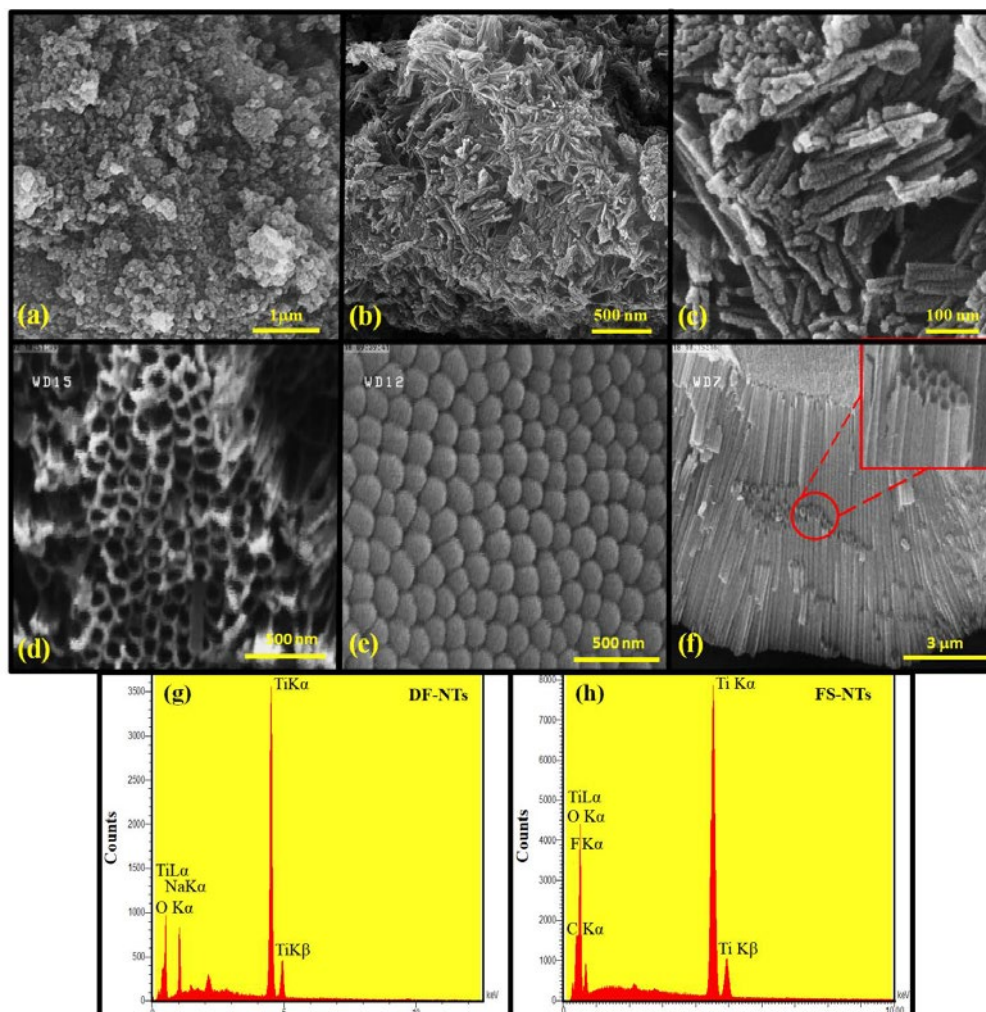


Fig. 2. FESEM images corresponding to (a) P25, (b,c) DF-NTs and (d-f) FS-NTs; and the EDS spectrum of (g) DF-NTs and (h) FS-NTs.

formed with tubular morphology and a layered shape. The DF-NTs have a diameter of 5-10 nm and length of several hundred nanometers, as presented in Fig. 2(b) and 2(c). Fig. 2(d) and 2(e) shows a top-view and barrier layer images corresponding to FS-NTs, respectively. It can be observed that the FS-NTs are well open at the top end and closed at the bottom. Based on the top view image in Fig. 2(d), the FS-NTs have an average internal diameter of about 75 nm and wall thickness of 15 nm, respectively. The cross-sectional FESEM image of the FS-NTs, as presented in Fig 2(f), shows the formation of tubular arrays with ordered and aligned structures through the two-step anodization procedure. Based on Fig. 2(f), FS-NTs have an average length about 8 μm. The elemental relative compositions of DF-NTs and FS-NTs acquired from EDS analysis are illustrated in Fig. 2 (g) and 2(h). Fig. 2(g) and 2(h) clearly show that the peaks corresponding to Ti and O are the prominent peaks in both spectra. Based on Fig. 2(g), it can be found that DF-NTs mainly consisted of Ti and O atoms which the weight contribution of titanium and oxygen was 51.27% and 41.52%, respectively. Both the elements together contributed 92.79% of the total weight. The very small remaining percentage in DF-NTs catalyst is ascribed to the existence of residual Na<sup>+</sup> ions that not be replaced by the H<sup>+</sup> ions provided from the acid treatment process. Based on Fig. 2(h), FS-NTs mainly consisted of Ti (42.92 wt%) and O (41.57

wt%) with some impurity including C and F. The existence of residual contaminants like carbon and fluorine is ascribed to the precursors, i.e. ethylene glycol and ammonium fluoride, respectively.

#### XRD measurements

The XRD patterns corresponding to the annealed commercial TiO<sub>2</sub> powder, DF-NTs and FS-NTs are shown in Fig. 3, respectively. All XRD patterns confirm the crystalline nature of the as-prepared catalysts and also indicate the existence of anatase phase (JCPDS-21-1272), as expected for TiO<sub>2</sub> nanotubes annealed at the 450 °C. Regarding Fig. 3, the diffraction peaks which were observed at 25.3°, 37.9°, 48.1°, 53.8°, 55.2°, 62.2°, 68.8°, 70.02° and 75.09° realize nanocrystalline of the anatase phase that can be indexed to the (101), (004), (200), (105), (211), (213), (116), (220) and (215) planes, respectively [36]. The average crystallite size of the fabricated samples was calculated based on the line broadening of the XRD peak observed around 25.3°, i.e. the (101) plane, using the Scherer's equation [37-40]:

$$D = \frac{k\lambda}{\beta \cos \theta} \quad (2)$$

where D is the average crystallite size, k is a constant (=0.89, here), λ is the wavelength of the X-ray radiation source (=1.5406 Å), θ is the Bragg's angle, and β is full width of the diffraction peak at half its maximum intensity in radian. Furthermore,

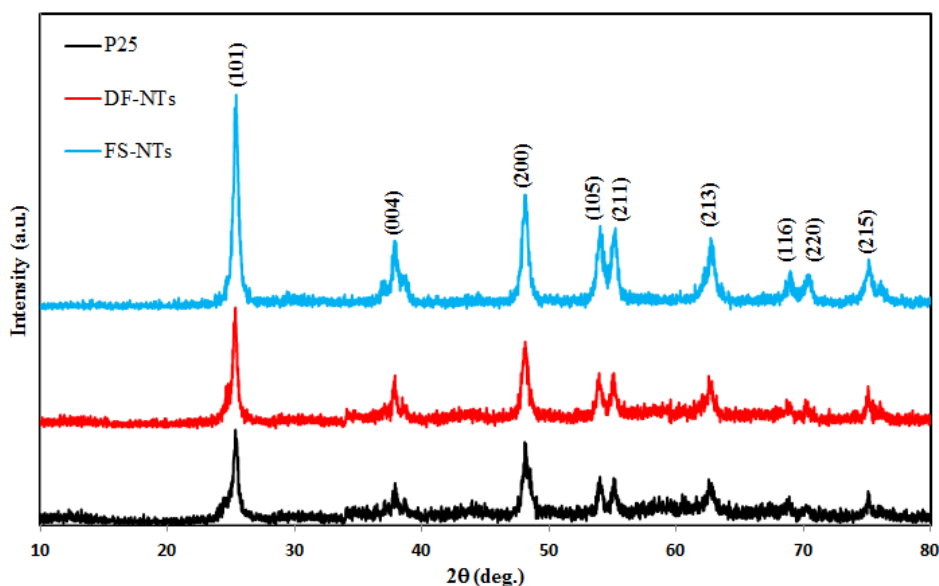


Fig. 3. XRD patterns corresponding to the annealed P25, DF-NTs and FS-NTs.

the lattice parameters were estimated using the following equations [41,42]:

$$\text{Bragg's law : } 2d_{(hkl)} \sin \theta = \lambda \quad (3)$$

$$\frac{1}{d_{(hkl)}^2} = \frac{h^2}{a^2} + \frac{k^2}{b^2} + \frac{l^2}{c^2} \quad (4)$$

where h, k and l are the crystal plane indices,  $d_{(hkl)}$  is the distance between the (hkl) crystal planes,  $\theta$  is the diffraction angle of the (hkl) crystal plane, and a, b, and c are lattice parameters (anatase crystal:  $a = b \neq c$ ). Also, volume of the crystal cells (tetragonal) was calculated through Equation (5).

$$v = a^2c \quad (5)$$

The calculated crystal sizes, lattice parameters and cell volumes of the fabricated catalysts are presented in Table 1. Regarding Table 1, the values of the lattice parameters are in line with the anatase structure of TiO<sub>2</sub> (JCPDS card 21-1272). Also, the crystallite size and the cell volume of all

samples are similar which their values are in the range of 20 nm and 134 Å<sup>3</sup>, respectively. These results could infer that there is no impurity in the TiO<sub>2</sub> crystalline lattices.

#### FTIR analysis

The FTIR was used to determine the functional groups that present in synthesized catalysts as presented in Fig. 4. The peaks found at about 3420 cm<sup>-1</sup> and 2962 cm<sup>-1</sup> are assigned to the Ti-OH bond [36]. For all the catalysts, the spectra indicate a roughly strong band at about 1635 cm<sup>-1</sup> to 1622 cm<sup>-1</sup> which are because of the OH bending vibration corresponding to chemisorbed and/or physisorbed water molecule on the catalysts surface [43]. The broad absorption peaks from 800 cm<sup>-1</sup> to 700 cm<sup>-1</sup> and 490 cm<sup>-1</sup> to 433 cm<sup>-1</sup> are ascribed to the asymmetric stretching, symmetric stretching, and the bending modes of Ti-O-Ti bond, respectively [44]. For all catalysts, a small band observed near 3780 cm<sup>-1</sup> is related to O-H stretching corresponding to the hydroxyl group to Ti atoms [45]. Also, FTIR spectra are represented several types of vibrations at 1100 cm<sup>-1</sup> to 1360

Table 1. Phase, crystal size and lattice parameters of the prepared catalysts

Catalysts	Crystal phase	Crystallite size (nm)	a=b (Å)	c (Å)	v (Å <sup>3</sup> )
P25	Anatase	20.11	3.77	9.45	134.31
DF-NTs	Anatase	20.11	3.77	9.46	134.45
FS-NTs	Anatase	20.12	3.77	9.48	134.74

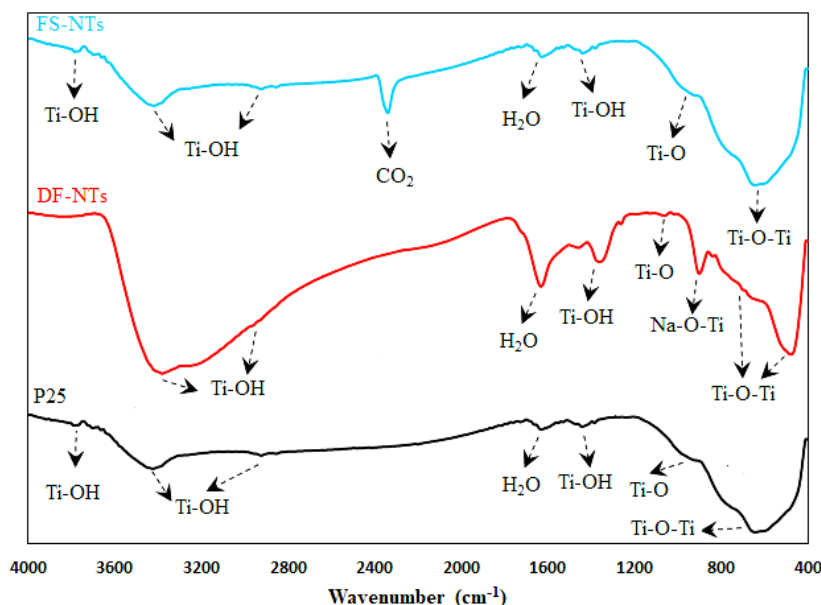


Fig. 4. FTIR spectra corresponding to DF-NTs and FS-NTs.

that they are assigned to the Ti-O stretching and Ti-OH bond, respectively [36]. The low-intensity broad band at around the 840 cm<sup>-1</sup> for DF-NTs sample is indicative of the Na-O bending of the Na-O-Ti bond of sodium titanates [46]. These results confirmed that P25, DF-NTs and FS-NTs are mainly consisted of Ti and O species which is well in agree with EDS results.

**BET measurements**

Specific surface areas, pore volume and average pore diameter of the catalysts were determined using the BET process analysis under N<sub>2</sub> adsorptive gas, as shown in Fig. 5. Table 2 presents the BET surface area and the corresponding pore volume for catalysts. Based on Fig. 5 (a) and 5 (b), the DF-NTs catalyst presented type IV isotherms with H3 type hysteresis loop at the relative pressure (P/P<sub>0</sub>) range of 0.4-1, based on the IUPAC classification [47], with the mean pore diameter of 9.54 nm. This result reflects the slit-like mesoporous geometry of DF-NTs catalyst. The slit-like pore geometry formed by DF-NTs is due to their aggregation and filament arrangement, which is expected for mesoporous materials [48]. According to Fig. 5 (c) and 5 (d) The as-synthesized FS-NTs catalyst

showed a type IV isotherm with H1 hysteresis loop in the relative pressure (P/P<sub>0</sub>) range of 0.4–1 and the average pore diameter was 11.75 nm, demonstrating the characteristics corresponding to mesoporous compounds. The H1 hysteresis loop of FS-NTs catalyst suggests a narrow range of uniform mesopores in the cylindrical pores form, which is in excellent accordance with the oriented tubular structures of FS-NTs. According to Table 2, both FS-NTs and DF-NTs have the highest surface area and pore volume than that commercial TiO<sub>2</sub> powder. Furthermore, the BET surface area (112.77 m<sup>2</sup>/g) and the related pore volume (0.34 cm<sup>3</sup>/g) of FS-NTs is considerably largest comparing to the surface area (86.54 m<sup>2</sup>/g) and pore volume (0.25 cm<sup>3</sup>/g) of DF-NTs. It is worth notable that in catalytic applications, the catalyst surface area is essential to provide enough active places for the reagents to react. In the current study, since

Table 2. Surface area and total pore volume corresponding to the different catalysts

Catalysts	Surface area (m <sup>2</sup> /g)	Pore volume (cm <sup>3</sup> /g)
P25	50	0.16
DF-NTs	86.54	0.25
FS-NTs	112.77	0.34

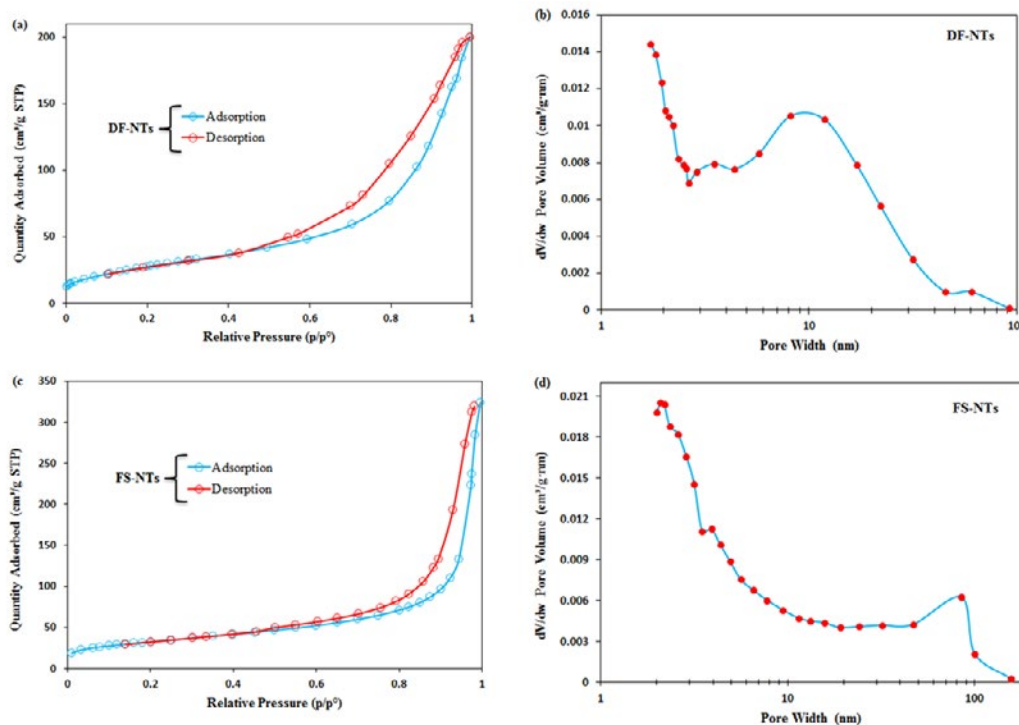


Fig. 5. (a) N<sub>2</sub> adsorption-desorption isotherms and (b) pore distribution of DF-NTs; (c) N<sub>2</sub> adsorption-desorption isotherms and (d) pore distribution of FS-NTs.



the FS-NTs catalysts have the highest surface area comparing to that two other catalysts, so we expect the FS-NTs catalysts show the higher catalytic behavior in generating hydrogen from the NaBH<sub>4</sub> solution.

*Investigation catalysts activity and hydrolysis mechanism*

The catalytic behavior of three different nanostructures, namely commercial TiO<sub>2</sub> powder, DF-NTs and FS-NTs, were investigated through measurement of the volume of hydrogen generated through hydrolyzing an alkaline NaBH<sub>4</sub> solution. The results of these experiments are presented in Fig. 6. After adding the catalysts, the hydrogen was released immediately without

any induction period. The rates of hydrogen generation (ml.min<sup>-1</sup>) were calculated from the fitting lines slopes that were achieved from the Volume-time curves. Fig. 6, showed that TiO<sub>2</sub> in three different nanostructures itself has catalytic activity for producing hydrogen. Previous studies indicated that there are two kinds of acid sites on the surface of TiO<sub>2</sub> nanotubes, namely Brønsted-acid sites (surface-bound hydroxyl group i.e. Ti-OH) and Lewis-acid sites (exposed Ti<sup>n+</sup> cation) [27,28]. Since NaBH<sub>4</sub> hydrolysis can catalyze by acid sites [29,30], so TiO<sub>2</sub> nanotubes can be added to reduce the activation energy and accelerate the generation of hydrogen. The hydrolysis reactions of sodium borohydride in existence of catalysts proceed via a seven-step reaction mechanism as

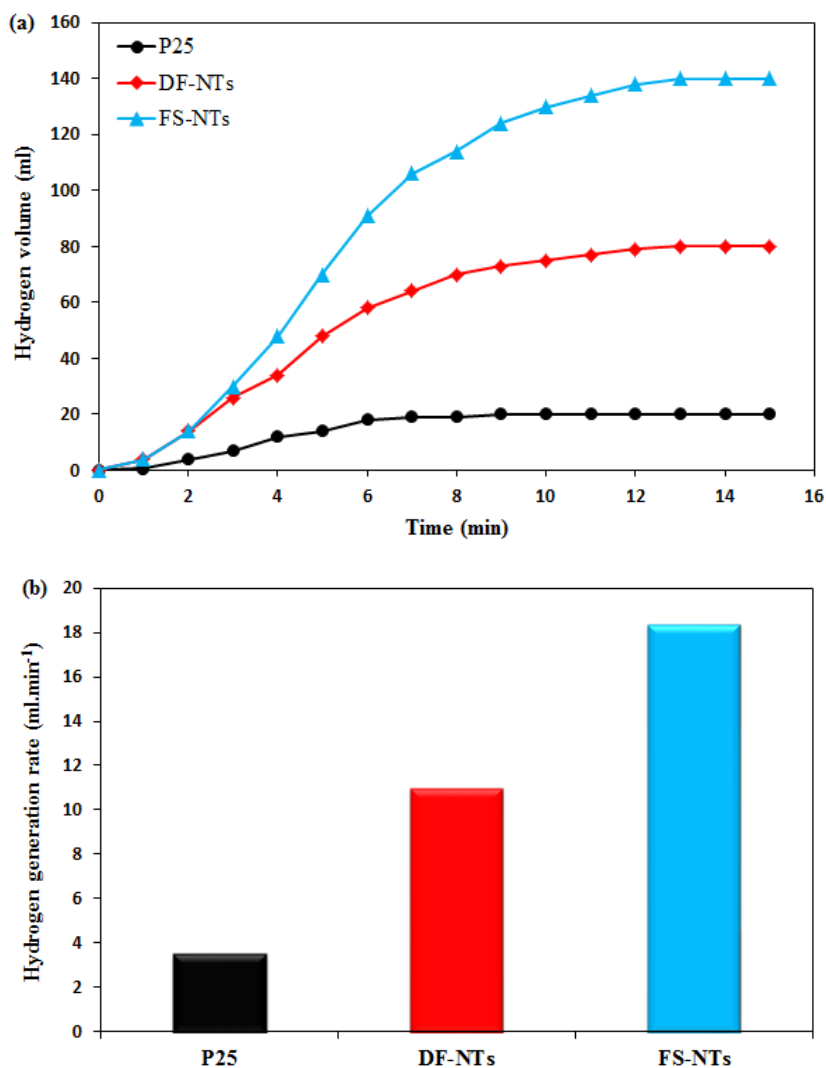
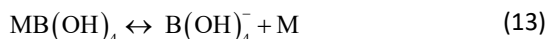
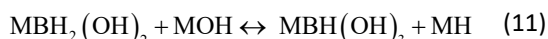


Fig. 6. The influence of different catalysts on (a) volume of generated hydrogen and (b) rate of generating hydrogen.

presented in reactions (2)–(9) [9,49]:



In the aforementioned reactions, the M symbol illustrates the TiO<sub>2</sub> catalysts. Based on the reactions above, we proposed a schematic illustration to clarify the mechanism of the hydrogen evolution from the catalytic hydrolysis of NaBH<sub>4</sub>, which is demonstrated in Fig. 7. The first step of the reaction is reversible chemisorption of borohydride ions (BH<sub>4</sub><sup>-</sup>) and H<sub>2</sub>O molecules to the active sites of TiO<sub>2</sub> atoms, respectively (reaction (2) and (3)). In the second step, a proton on the borohydride ion then exchanges with a hydroxide ion to form M-H and comparatively stable intermediate BH<sub>3</sub>(OH)<sup>-</sup> based on reaction (4). Simultaneously, hydridic H<sup>-</sup> of BH<sub>4</sub><sup>-</sup> reacts with protic hydrogen of H<sub>2</sub>O leads to the generation H<sub>2</sub> as represented by reaction (5). The generated intermediate ion (BH<sub>3</sub>(OH)<sup>-</sup>) is expected to have similar reactivity as borohydride ion and the cycle of charge transfer goes through similar steps as BH<sub>3</sub>(OH)<sup>-</sup> → BH<sub>2</sub>(OH)<sub>2</sub><sup>-</sup> → BH(OH)<sub>3</sub><sup>-</sup> → B(OH)<sub>4</sub><sup>-</sup>, releasing H<sub>2</sub> at each step (reaction (6)–(9)).

By comparing two different TiO<sub>2</sub> nanotubes

with commercial TiO<sub>2</sub> powder, it can be observed both DF-NTs and FS-NTs catalysts improved the hydrogen generation rates from 3.5 ml.min<sup>-1</sup> (for TiO<sub>2</sub> powder) to 11 ml.min<sup>-1</sup> (for DF-NTs) and 18.4 (for FS-NTs) ml.min<sup>-1</sup>, respectively. Based on Fig. 6, FS-NTs catalyst showed better catalytic activity than the DF-NTs catalyst which it could cause more than 1.5-fold improvement on the hydrogen generation volume and rate from 80 to 140 ml and from 11 to 18.4 ml.min<sup>-1</sup>, respectively. This remarkable enhancement in catalytic activity of FS-NTs than DF-NTs catalyst can result from two factors. Firstly, based on Table 2, FS-NTs have the highest surface area than that DF-NTs catalyst. It is evident that the catalyst surface area and its catalytic performance are only related together indirectly. A catalyst with the larger surface area is assumed to have more exposed catalytically active places comparing to the same catalyst with the smaller surface area. Hence FS-NTs catalyst showed better catalytic performance than two other catalysts in hydrogen generation as a result of the improvement in the surface area. Secondly, more orderliness and oriented structure of FS-NTs than DF-NTs catalyst lead to easily transfer of reagents and more adsorbed on the nanotubes surfaces. More adsorption of reagents on reactive sites causes more accelerations of catalytic hydrolysis rate and consequently generates more hydrogen over FS-NTs catalysts.

#### Kinetic study of the catalytic hydrolysis of NaBH<sub>4</sub>

To investigate the kinetic properties of the catalytic hydrolysis of NaBH<sub>4</sub> with FS-NTs catalysts, the reaction rates were studied as a function of catalyst concentration and amount of NaBH<sub>4</sub>. The influence of NaBH<sub>4</sub> level on the rate of hydrogen generation was examined with various initial levels of NaBH<sub>4</sub> ranging from 1 wt% to 10 wt% while the

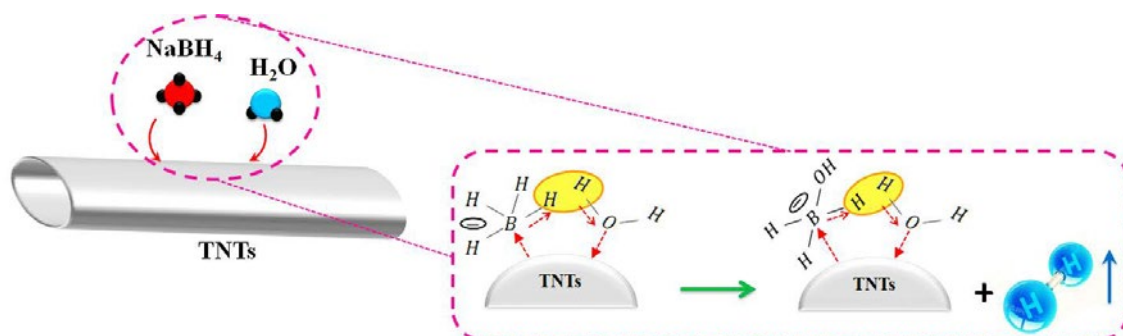


Fig. 7. Proposed mechanism for the catalytic hydrolysis of NaBH<sub>4</sub> by TiO<sub>2</sub> nanotubes.

constant level of NaOH (1.5 wt%) was used. Fig. 8(a) represents the diagram corresponding to the volume of hydrogen generated versus time over the hydrolysis of NaBH<sub>4</sub> using diverse initial NaBH<sub>4</sub> concentrations at 30 °C. The volume of generated hydrogen increased by rising up the NaBH<sub>4</sub> concentration from 1 wt.% to 5 wt.%, and next it started to reduce regarding the rise of initial NaBH<sub>4</sub> concentration to 10 wt.%. This phenomenon can be explained by the way that when the NaBH<sub>4</sub> level is lower than the value where the maximum rate of hydrogen generation is obtained, more BH<sub>4</sub><sup>-</sup> and H<sub>2</sub>O can contact the active place on catalyst surface to generate hydrogen at higher NaBH<sub>4</sub> concentration. However, it should be noticed that NaBO<sub>2</sub> is produced simultaneously with hydrogen, and higher initial NaBH<sub>4</sub> concentration can lead to more NaBO<sub>2</sub> accumulated on the surface of catalyst and in the solution because of the low solubility of NaBO<sub>2</sub> in alkaline solution. Consequently, the catalytic active places on the catalyst will be blocked, the solution viscosity will increase and the mass transfer will be impeded [23, 50]. Fig. 8(b) shows the diagrams corresponding to the rate of hydrogen generation versus NaBH<sub>4</sub>

concentration, both in logarithmic scales. The slope corresponding to the resultant straight line is observed to be 0.0155, which is close to zero, implying that the NaBH<sub>4</sub> catalytic hydrolysis over FS-NTs is a zero-order reaction regarding the concentration of NaBH<sub>4</sub>.

The influence of catalyst concentration on generating hydrogen for the catalytic hydrolysis of NaBH<sub>4</sub> using FS-NTs was further investigated by performing a set of control experiments using diverse levels of FS-NTs catalysts in a range of 50-200 mg while the other reaction conditions were constant. Fig. 8(c) indicates the plot corresponding to the hydrogen generation volume versus time for hydrolyzing NaBH<sub>4</sub> using diverse initial catalyst amount at 30 °C. As shown in Fig. 8(c), increasing the catalyst amount could promote the rate of reaction apparently. Based on the Fig. 7(c), as the amount of the catalyst was enhanced from 50 to 200 mg, the hydrogen generation volume increased from 56 mL to 216 mL after 15 min of reaction. Fig. 8(d) illustrate the diagram corresponding to the rate of hydrogen generation versus FS-NTs amount, both in logarithmic scales. As shown in Fig. 8(d), the catalytic rate exhibits

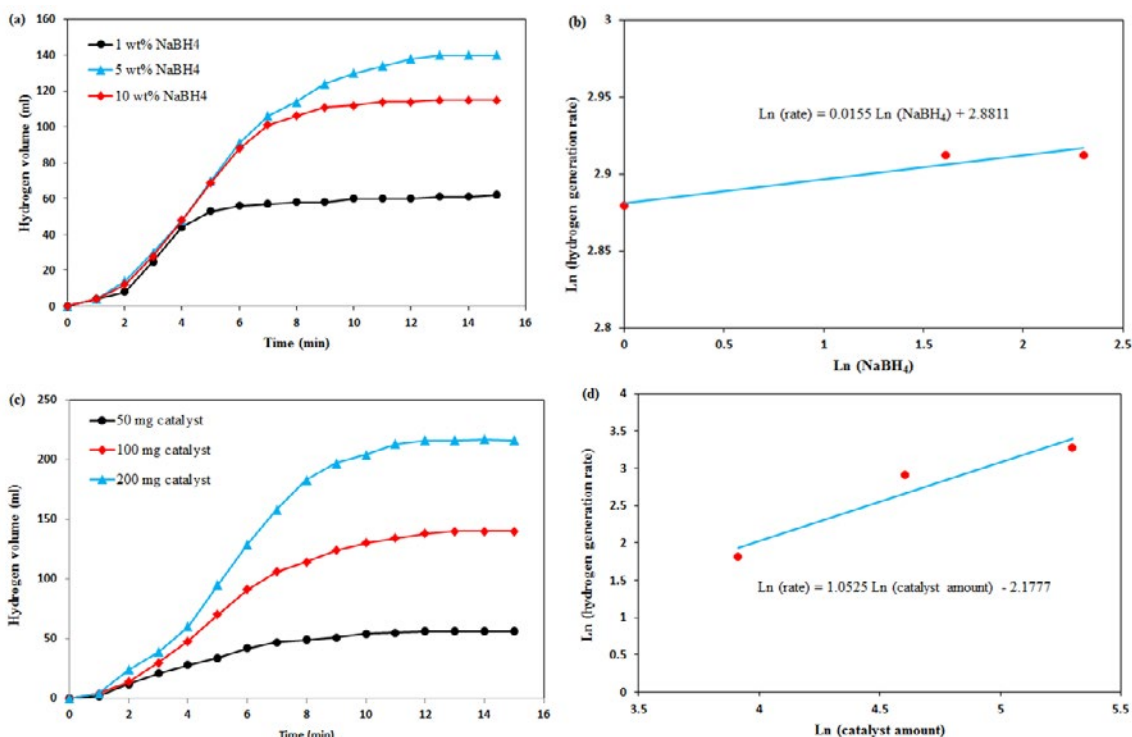


Fig. 8. (a) Effect of NaBH<sub>4</sub> concentration on hydrogen generation and (b) Ln (hydrogen generation rate) as a function Ln (NaBH<sub>4</sub>); (c) Influence of catalyst amount on hydrogen generation and (d) Ln (hydrogen generation rate) as a function Ln (catalyst amount).

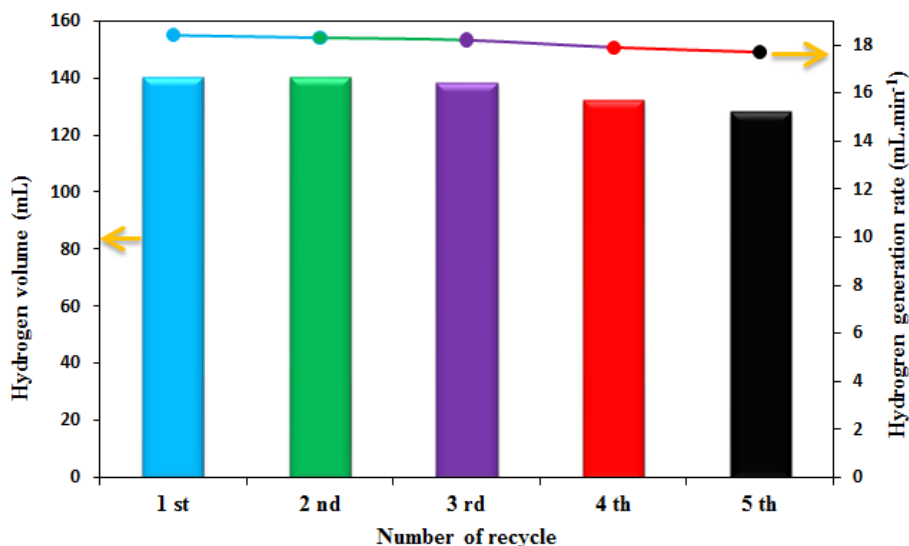


Fig. 9. The FS-NTs catalyst reusability for hydrolyzing NaBH<sub>4</sub>.

a linear growth with catalyst amount. Achieving a fitted straight line with a slope very close to 1 (1.05) demonstrated that hydrolyzing NaBH<sub>4</sub> using the catalyst of FS-NTs is a first-order reaction respecting to the concentration of the catalyst.

Hence as a result of the kinetic study, the rate law for hydrolyzing of NaBH<sub>4</sub> over using the catalyst of FS-NTs under our reaction conditions can be represented as follows:

$$r = \frac{d[H_2]}{dt} = -4 \frac{d[NaBH_4]}{dt} = k[FS-NTs]^{1.05} \quad (14)$$

$$[NaBH_4]^{0.016} \approx k[FS-NTs]$$

Where *r* is the rate of reaction and *k* represents the rate constant. This equation is in good agreement with the results reported by Shen et al. for an Ag-activated TiO<sub>2</sub> catalyst [26], by Cheng et al. for a Co-B-TiO<sub>2</sub> catalyst [25], and by Rakap et al. for a Co-Ni-P/Pd-TiO<sub>2</sub> catalyst [3].

#### Reusability

The durability and recyclability of a catalyst is another important parameter which determines its potential in practical hydrogen generation systems. The durability and reusability of FS-NTs for generating hydrogen from NaBH<sub>4</sub> were evaluated in aqueous solution up to the fifth run at 30 °C. Fig. 9 represents the volumes of generated hydrogen and the rates of hydrogen generation. The catalytic performance of FS-NTs in hydrogen generation

volumes remained almost unchanged, preserving 87% of its initial catalytic performance after five cycles. As shown in Fig. 9, no significant decay in the rate of hydrogen generation was observed even after fifth runs in the reusability test, which demonstrates the superior catalytic durability of FS-NTs to accelerate the NaBH<sub>4</sub> hydrolysis.

#### CONCLUSION

In summary, the generating hydrogen from the catalytic hydrolysis of NaBH<sub>4</sub> as a function of TiO<sub>2</sub> nanostructures was examined. For this purpose, DF-NTs and FS-NTs were prepared via the hydrothermal and chemical-assisted two-step anodization processes, respectively. The FESEM results confirmed that hydrothermal method leads to preparation of disordered filaments TiO<sub>2</sub> nanotubes while chemical-assisted two-step anodization method causes the production of ordered free-standing TiO<sub>2</sub> nanotubes. Furthermore, the BET results showed that the FS-NTs catalyst has the highest specific surface area (112.77 m<sup>2</sup>/g) which it was 1.30 and 2.25 times greater than that DF-NTs (86.54 m<sup>2</sup>/g) and spherical TiO<sub>2</sub> (50 m<sup>2</sup>/g) samples, respectively. As a result of enhancement in the specific surface area, the FS-NTs catalysts showed preferable activity in the hydrogen generation comparing with the two other catalysts. In this regard, FS-NTs could generate 140 ml H<sub>2</sub> with the rate 18.4 ml.min<sup>-1</sup> that it was 1.75 and 7 times more than the volume corresponding to generated H<sub>2</sub> by DF-

NTs and spherical TiO<sub>2</sub>, respectively. Moreover, the kinetic studies indicated that the NaBH<sub>4</sub> catalytic hydrolysis by FS-NTs was a first-order reaction regarding the catalyst weight, whereas it was a zero-order reaction as a function of NaBH<sub>4</sub> concentration. Furthermore, the FS-NTs catalyst revealed good stability and was reused for five runs without the significant loss of catalytic performance. To sum up, this research exhibited that using free-standing TiO<sub>2</sub> nanotubes as a potent support catalyst can dramatically increase the rate of generating hydrogen from NaBH<sub>4</sub> catalytic hydrolysis application.

#### CONFLICT OF INTEREST

The authors declare that there are no conflicts of interest regarding the publication of this manuscript.

#### REFERENCES

- Ghiyasiyan-Arani M, Salavati-Niasari M. Effect of Li<sub>2</sub>CoMn<sub>3</sub>O<sub>8</sub> Nanostructures Synthesized by a Combustion Method on Montmorillonite K10 as a Potential Hydrogen Storage Material. *The Journal of Physical Chemistry C*. 2018;122(29):16498-509.
- Salehabadi A, Salavati-Niasari M, Ghiyasiyan-Arani M. Self-assembly of hydrogen storage materials based multi-walled carbon nanotubes (MWCNTs) and Dy<sub>3</sub>Fe<sub>5</sub>O<sub>12</sub> (DFO) nanoparticles. *Journal of Alloys and Compounds*. 2018;745:789-97.
- Salehabadi A, Sarrami F, Salavati-Niasari M, Gholami T, Spagnoli D, Karton A. Dy<sub>3</sub>Al<sub>2</sub>(AlO<sub>4</sub>)<sub>3</sub> ceramic nanogarnets: Sol-gel auto-combustion synthesis, characterization and joint experimental and computational structural analysis for electrochemical hydrogen storage performances. *Journal of Alloys and Compounds*. 2018;744:574-82.
- Razavi FS, Morassaei MS, Salehabadi A, Ghiyasiyan-Arani M, Salavati-Niasari M. Structural characterization and electrochemical hydrogen sorption performances of the polycrystalline Ba<sub>2</sub>Co<sub>9</sub>O<sub>14</sub> nanostructures. *Journal of Alloys and Compounds*. 2019;777:252-8.
- Salehabadi A, Salavati-Niasari M, Gholami T. Green and facial combustion synthesis of Sr<sub>3</sub>Al<sub>2</sub>O<sub>6</sub> nanostructures; a potential electrochemical hydrogen storage material. *Journal of Cleaner Production*. 2018;171:1-9.
- Alenzi N, Liao W-S, Cremer PS, Sanchez-Torres V, Wood TK, Ehlig-Economides C, et al. Photoelectrochemical hydrogen production from water/methanol decomposition using Ag/TiO<sub>2</sub> nanocomposite thin films. *International Journal of Hydrogen Energy*. 2010;35(21):11768-75.
- Hakamizadeh M, Afshar S, Tadjarodi A, Khajavian R, Fadaie MR, Bozorgi B. Improving hydrogen production via water splitting over Pt/TiO<sub>2</sub>/activated carbon nanocomposite. *International Journal of Hydrogen Energy*. 2014;39(14):7262-9.
- Fan M-Q, Liu S, Sun WQ, Fei Y, Pan H, Shu K-Y. Controllable hydrogen generation and hydrolysis mechanism of AlLi/NaBH<sub>4</sub> system activated by CoCl<sub>2</sub> solution. *Renewable Energy*. 2012;46:203-9.
- Manna J, Roy B, Pareek D, Sharma P. Hydrogen generation from NaBH<sub>4</sub> hydrolysis using Co-B/AlPO<sub>4</sub> and Co-B/bentonite catalysts. *Catalysis, Structure & Reactivity*. 2017;3(4):157-64.
- Shu C, Sun T, Jia J, Lou Z. Mild Process for Reductive Desulfurization of Diesel Fuel Using Sodium Borohydride in Situ Generated via Sodium Metaborate Electroreduction. *Industrial & Engineering Chemistry Research*. 2013;52(23):7660-7.
- Brack P, Dann SE, Wijayantha KGU. Heterogeneous and homogenous catalysts for hydrogen generation by hydrolysis of aqueous sodium borohydride (NaBH<sub>4</sub>) solutions. *Energy Science & Engineering*. 2015;3(3):174-88.
- Demirci UB, Miele P. Cobalt in NaBH<sub>4</sub> hydrolysis. *Physical Chemistry Chemical Physics*. 2010;12(44):14651.
- Wang MC, Ouyang LZ, Liu JW, Wang H, Zhu M. Hydrogen generation from sodium borohydride hydrolysis accelerated by zinc chloride without catalyst: A kinetic study. *Journal of Alloys and Compounds*. 2017;717:48-54.
- Lin K-YA, Chang H-A. Efficient hydrogen production from NaBH<sub>4</sub> hydrolysis catalyzed by a magnetic cobalt/carbon composite derived from a zeolitic imidazolate framework. *Chemical Engineering Journal*. 2016;296:243-51.
- Ma X, Ye K, Wang G, Duan M, Cheng K, Wang G, et al. Facile fabrication of gold coated nickel nanoarrays and its excellent catalytic performance towards sodium borohydride electro-oxidation. *Applied Surface Science*. 2017;414:353-60.
- Chowdhury AD, Agnihotri N, De A. Hydrolysis of sodium borohydride using Ru-Co-PEDOT nanocomposites as catalyst. *Chemical Engineering Journal*. 2015;264:531-7.
- Ma Y, Li X, Zhang Y, Chen L, Wu J, Gao D, et al. Ruthenium nanoparticles supported on TiO<sub>2</sub> (B) nanotubes: Effective catalysts in hydrogen evolution from the hydrolysis of ammonia borane. *Journal of Alloys and Compounds*. 2017;708:270-7.
- Liang Z, Xiao X, Yu X, Huang X, Jiang Y, Fan X, et al. Non-noble trimetallic Cu-Ni-Co nanoparticles supported on metal-organic frameworks as highly efficient catalysts for hydrolysis of ammonia borane. *Journal of Alloys and Compounds*. 2018;741:501-8.
- Loghmani MH, Shojaei AF, Khakzad M. Hydrogen generation as a clean energy through hydrolysis of sodium borohydride over Cu-Fe-B nano powders: Effect of polymers and surfactants. *Energy*. 2017;126:830-40.
- Şahin Ö, Kılınc D, Saka C. Bimetallic Co-Ni based complex catalyst for hydrogen production by catalytic hydrolysis of sodium borohydride with an alternative approach. *Journal of the Energy Institute*. 2016;89(4):617-26.
- Eugénio S, Demirci UB, Silva TM, Carmezim MJ, Montemor MF. Copper-cobalt foams as active and stable catalysts for hydrogen release by hydrolysis of sodium borohydride. *International Journal of Hydrogen Energy*. 2016;41(20):8438-48.
- Chaugule AA, Tamboli AH, Sheikh FA, Kim H. Preparation and application of Sm-Ni oxide doped TiO<sub>2</sub> nanofiber as catalyst in hydrogen production from sodium borohydride hydrolysis. *Colloids and Surfaces A: Physicochemical and Engineering Aspects*. 2015;484:242-52.
- Şahin Ö, İzgi MS, Onat E, Saka C. Influence of the using of methanol instead of water in the preparation of Co-B-TiO<sub>2</sub> catalyst for hydrogen production by NaBH<sub>4</sub> hydrolysis and plasma treatment effect on the Co-B-TiO<sub>2</sub> catalyst. *International Journal of Hydrogen Energy*. 2016;41(4):2539-46.
- Xiang C, Jiang D, She Z, Zou Y, Chu H, Qiu S, et al. Hydrogen

- generation by hydrolysis of alkaline sodium borohydride using a cobalt–zinc–boron/graphene nanocomposite treated with sodium hydroxide. *International Journal of Hydrogen Energy*. 2015;40(11):4111-8.
25. Dadkhah M, Salavati-Niasari M, Mir N. Synthesis and characterization of TiO<sub>2</sub> nanoparticles by using new shape controllers and its application in dye sensitized solar cells. *Journal of Industrial and Engineering Chemistry*. 2014;20(6):4039-44.
  26. Masjedi M, Mir N, Noori E, Gholami T, Salavati-Niasari M. Effect of Schiff base ligand on the size and the optical properties of TiO<sub>2</sub> nanoparticles. *Superlattices and Microstructures*. 2013;62:30-8.
  27. Bhattacharyya K, Danon A, K.Vijayan B, Gray KA, Stair PC, Weitz E. Role of the Surface Lewis Acid and Base Sites in the Adsorption of CO<sub>2</sub> on Titania Nanotubes and Platinized Titania Nanotubes: An in Situ FT-IR Study. *The Journal of Physical Chemistry C*. 2013;117(24):12661-78.
  28. Harima Y, Fujita T, Kano Y, Imae I, Komaguchi K, Ooyama Y, et al. Lewis-Acid Sites of TiO<sub>2</sub> Surface for Adsorption of Organic Dye Having Pyridyl Group as Anchoring Unit. *The Journal of Physical Chemistry C*. 2013;117(32):16364-70.
  29. Ramya K, Dhathathreyan KS, Sreenivas J, Kumar S, Narasimhan S. Hydrogen production by alcoholysis of sodium borohydride. *International Journal of Energy Research*. 2013;37(14):1889-95.
  30. Shang Y, Chen R, Jiang G. Kinetic study of NaBH<sub>4</sub> hydrolysis over carbon-supported ruthenium. *International Journal of Hydrogen Energy*. 2008;33(22):6719-26.
  31. Bandal HA, Jadhav AR, Kim H. Cobalt impregnated magnetite-multiwalled carbon nanotube nanocomposite as magnetically separable efficient catalyst for hydrogen generation by NaBH<sub>4</sub> hydrolysis. *Journal of Alloys and Compounds*. 2017;699:1057-67.
  32. Chen S, Ostrom C, Chen A. Functionalization of TiO<sub>2</sub> nanotubes with palladium nanoparticles for hydrogen sorption and storage. *International Journal of Hydrogen Energy*. 2013;38(32):14002-9.
  33. Pang YL, Lim S, Ong HC, Chong WT. A critical review on the recent progress of synthesizing techniques and fabrication of TiO<sub>2</sub>-based nanotubes photocatalysts. *Applied Catalysis A: General*. 2014;481:127-42.
  34. Pasikhani JV, Gilani N, Pirbazari AE. The effect of the anodization voltage on the geometrical characteristics and photocatalytic activity of TiO<sub>2</sub> nanotube arrays. *Nano-Structures & Nano-Objects*. 2016;8:7-14.
  35. Pasikhani JV, Gilani N, Pirbazari AE. The correlation between structural properties, geometrical features, and photoactivity of freestanding TiO<sub>2</sub> nanotubes in comparative degradation of 2,4-dichlorophenol and methylene blue. *Materials Research Express*. 2018;5(2):025016.
  36. Pasikhani JV, Gilani N, Pirbazari AE. Improvement the wastewater purification by TiO<sub>2</sub> nanotube arrays: The effect of etching-step on the photo-generated charge carriers and photocatalytic activity of anodic TiO<sub>2</sub> nanotubes. *Solid State Sciences*. 2018;84:57-74.
  37. Namvar F, Sadat Sangsefidi F, Salavati-Niasari M. Tb<sub>2</sub>MoO<sub>6</sub> nanostructure: Ultrasonic controlling the size and morphology, characterization and investigation of its photo-catalytic activity for dyes as the water pollutants under UV light illumination. *Journal of Hazardous Materials*. 2018;360:288-302.
  38. Haghjoo H, Sangsefidi FS, Salavati-Niasari M. Synthesis and characterization of Pb<sub>2</sub>SiO<sub>4</sub> nanostructure: study of photo-catalytic behavior of reactive Red198 and reactive Orange16 dyes as pollutants. *Journal of Materials Science: Materials in Electronics*. 2018;29(10):8002-9.
  39. Haghjoo H, Sangsefidi FS, Salavati-Niasari M. Study on the optical, magnetic, and photocatalytic activities of the synthesized Mn<sub>2</sub>O<sub>3</sub>-SiO<sub>2</sub> nanocomposites by microwave method. *Journal of Molecular Liquids*. 2017;242:779-88.
  40. Haghjoo H, Sangsefidi FS, Salavati-Niasari M. Synthesis of PbSiO<sub>3</sub> nanoparticles in the presence of proteins as a greencapping agent and their application as photocatalyst. *Journal of Molecular Liquids*. 2017;247:345-53.
  41. Gilani N, Pasikhani JV, Motie PT, Akbari M. Fabrication of quantum Cu(II) nanodot decorated TiO<sub>2</sub> nanotubes by the photochemical deposition-assisted hydrothermal method: study catalytic activity in hydrogen generation. *DESALINATION AND WATER TREATMENT*. 2019;139:145-55.
  42. Haghjoo H, Sangsefidi FS, Hashemizadeh SA, Salavati-Niasari M. Investigation the magnetic properties and the photocatalytic activity of synthesized Mn<sub>7</sub>SiO<sub>12</sub> nanostructures by green capping agent. *Journal of Molecular Liquids*. 2017;225:290-5.
  43. Monsef R, Ghiyasiyan-Arani M, Salavati-Niasari M. Utilizing of neodymium vanadate nanoparticles as an efficient catalyst to boost the photocatalytic water purification. *Journal of Environmental Management*. 2019;230:266-81.
  44. Natarajan TS, Lee JY, Bajaj HC, Jo W-K, Tayade RJ. Synthesis of multiwall carbon nanotubes/TiO<sub>2</sub> nanotube composites with enhanced photocatalytic decomposition efficiency. *Catalysis Today*. 2017;282:13-23.
  45. Mazloom F, Ghiyasiyan-Arani M, Monsef R, Salavati-Niasari M. Photocatalytic degradation of diverse organic dyes by sol-gel synthesized Cd<sub>2</sub>V<sub>2</sub>O<sub>7</sub> nanostructures. *Journal of Materials Science: Materials in Electronics*. 2018;29(21):18120-7.
  46. Tsiourvas D, Tsetsekou A, Arkas M, Diplas S, Mastrogianni E. Covalent attachment of a bioactive hyperbranched polymeric layer to titanium surface for the biomimetic growth of calcium phosphates. *Journal of Materials Science: Materials in Medicine*. 2010;22(1):85-96.
  47. Thommes M, Kaneko K, Neimark AV, Olivier JP, Rodriguez-Reinoso F, Rouquerol J, et al. Physisorption of gases, with special reference to the evaluation of surface area and pore size distribution (IUPAC Technical Report). *Pure and Applied Chemistry*. 2015;87(9-10):1051-69.
  48. Labani MM, Rezaee R, Saeedi A, Hinai AA. Evaluation of pore size spectrum of gas shale reservoirs using low pressure nitrogen adsorption, gas expansion and mercury porosimetry: A case study from the Perth and Canning Basins, Western Australia. *Journal of Petroleum Science and Engineering*. 2013;112:7-16.
  49. Wu Z, Mao X, Zi Q, Zhang R, Dou T, Yip ACK. Mechanism and kinetics of sodium borohydride hydrolysis over crystalline nickel and nickel boride and amorphous nickel–boron nanoparticles. *Journal of Power Sources*. 2014;268:596-603.
  50. Li Z, Li H, Wang L, Liu T, Zhang T, Wang G, et al. Hydrogen generation from catalytic hydrolysis of sodium borohydride solution using supported amorphous alloy catalysts (Ni–Co–P/γ-Al<sub>2</sub>O<sub>3</sub>). *International Journal of Hydrogen Energy*. 2014;39(27):14935-41.